Solar Energy Materials & Solar Cells 94 (2010) 106–113

Contents lists available at ScienceDirect

Solar Energy Materials & Solar Cells

journal homepage: www.elsevier.com/locate/solmat

Review

Detection and analysis of hot-spot formation in solar cells

Michael Simon *, Edson L. Meyer

Fort Hare Institute of Technology, University of Fort Hare, Private Bag x1314, Alice 5700, South Africa

ARTICLE INFO

Article history:
Received 27 April 2009
Received in revised form
11 August 2009
Accepted 29 September 2009
Available online 22 October 2009

Keywords:
Hot-spot
Infrared thermography
Transitions metals

ABSTRACT

In this study, infrared thermography (IR) was used to map the surface temperature distribution of solar cells while in the reverse bias mode. It was observed that some cells exhibited an inhomogeneity of the surface temperature resulting in localized heating (hot-spot). Using the scanning electron microscopy (SEM), the structural images of hot-spot areas revealed that hot-spot heating causes irreversible destruction of the solar cell structure. Different techniques were later used to analyze the elemental composition of the different regions of the solar cells. It was revealed that a direct correlation exists between areas of high impurity contaminants and hot-spot heating. Areas with high concentration of transition metals resulted in hot-spot formation. The results of all the samples are presented in detail in this paper.

Contents

1. Introduction

Although some standardized accelerated tests for extreme outdoor environment are used for qualification tests procedures, failures in crystalline-Si modules or cells still occur. These failure modes arising from the intrinsic properties of c-Si may be due to casting techniques employed in the fabrication process. The variations and the complexity of the intrinsic properties of c-Si cells have forced many scientists and photovoltaic engineers to embark on a 'cause finding mission' with the ultimate goal of improving its efficiency and reliability, which has been compromised due to pre-mature failures. Wide research is the common phenomenon of hot-spots commonly associated with c-Si cells. Hot-spot heating in c-Si modules occurs when the modules' operating current exceeds the short-circuit (I_{sc}) of a low current producing cell [1,2]. The reduced I_{sc} of cells encapsulated in PV modules, becomes reverse biased, which leads to power dissipation resulting in the increase in surface temperature. Hot-spot heating is caused by various mechanisms e.g., shading or partial shading and shunting behavior of the cell's pn junction [3]. These localized shunting paths within a cell may be due to impurities accumulated on wafers during junction diffusion, or incomplete scribe lines [4]. Using an infrared (IR) thermography technique, hot-spot (which emits infrared radiation dependant on the temperature of the material) areas are easily and quickly located.

In this study IR thermography was used to locate hot-spot areas in different samples of solar cells. Some cells did not exhibit any hot-spot phenomenon. Three cells have been found to have areas of relatively high temperature ($\sim$150 °C) in certain locations within the cell. These high-temperature areas (hot-spot areas) have been analyzed using both scanning electron microscopy (SEM) and energy dispersive X-ray spectroscopy (EDX) analyses.

* Corresponding author. Tel: +27 40 602 2086; fax: +27 40 653 0665.
E-mail address: msimon@ufh.ac.za (M. Simon).

0927-0248/$ - see front matter © 2009 Elsevier B.V. All rights reserved.
doi:10.1016/j.solmat.2009.09.016

2. Hot-spot heating phenomenon

Hot-spot phenomenon in c-Si cells has been widely documented [5–7]. Although enormous work has been done in this regard, the understanding of this phenomenon is still far from complete. The reasons are partly due to different fabrication techniques employed by various solar cell manufacturers. Although research has attributed hot-spot regions in c-Si cells to various causes, the discrete presence of impurities in crystalline solar cells has not been linked to hot-spots. Due to inhomogeneity in the cells' current, the low-current producing cells in the module tends to operate under reverse bias, dissipating power in the form of heat. Fig. 1 illustrates the current–voltage (I–V) curve characteristics of a solar cell in both the forward and the reverse modes.

Clearly, an analysis of the I–V curve gives a lot of information with regards to hot-spot heating. Analyzing the slope of the I–V curve in the reverse bias mode gives information regarding the cell's pn junction properties and shunt paths [8]. Analyzing an I–V curve in Fig. 1, the decrease in shunt resistance (R_{sh}) has an effect on the I–V slope of a cell in the reverse direction, resulting in high-power dissipation. The dissipated power causes breakdown in localized regions of the junction leading to hot-spots. Although the use of an I–V curve is regarded as a simple tool for diagnosing flaws in PV modules or cell, one limiting factor is that it does not locate the defective cell that is dissipating heat as a result of reduced R_{sh}.

For solar-grade multicrystalline silicon (mc-Si) solar cells, metallic impurities are of great concern due to their detrimental effects on carrier lifetimes thereby compromising its efficiency [9]. These metal contaminants basically originate from the processing stages of mc-Si, in which case crystallization occurs from bottom to top of an ingot. During these crystallization stages, high impurity concentrations diffuse from the crucible at the bottom and form impurity segregation at the top [10].

Depending on the homogeneity of the metal contaminants, some contaminants appear as substitutional or interstitial ions in which case they can be alone or paired with dopants atoms [11]. The application of different gettering techniques has alleviated the problem and come as a solution for removing interstitial impurities in mc-Si. Work done in the past revealed that metal impurities affect negatively the efficiencies of cells especially in the regions of high minority carrier recombination. However, no work has attributed the presence of localized regions of high impurity concentrations to the formation of hot-spots.

The traditional understanding of shunt paths in a solar cell has been associated with an ohmic characteristic across the pn junction. With the use of infrared thermography, hot-spots can be located and not all shunts are ohmic in nature. Different shunt types in c-Si cell have been reported [12]. These shunt types are process-induced, caused by grown-in defects of the material. Process-induced shunts are due to residues of the emitter within the cell edge, cracks within the cell, and Schottky-type shunts just below grid lines. The process-induced shunts are due to strong recombination sites at grown-in defects and inversion layers caused by microscopic (SiC) precipitates on grain boundaries [13]. In an operational cell or module, these shunt types dissipate power in the form of heat, which if the dissipated heat is localized, overheating in a cell might occur resulting in solder melting or complete deterioration of the encapsulate. Fig. 2 illustrates an observed solder melt in a c-Si solar due to overheating (hot-spot) caused by Schottky-type shunts.

Shunt sites in c-Si have been observed to contain elevated amounts of transition metals, oxygen, and carbon. These impurities are inherent to the production processes of c-Si solar cells, which use low-grade material for low production cost. The presence of lower quantities of these transition metals enhances the insertion of new energy levels within the silicon band-gap, leading to poor performance of solar cell [14].

The effect of high concentration of transition metals, oxygen and carbon has not been correlated to hot-spot formation.

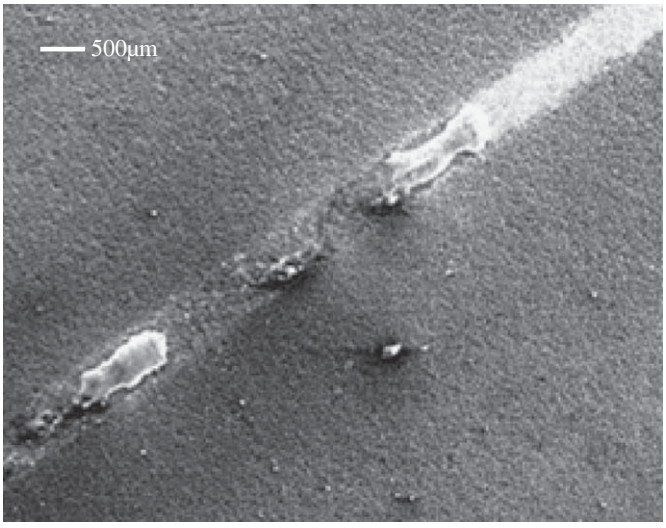

Fig. 2. Solder melt in mc-Si at hot-spot site.

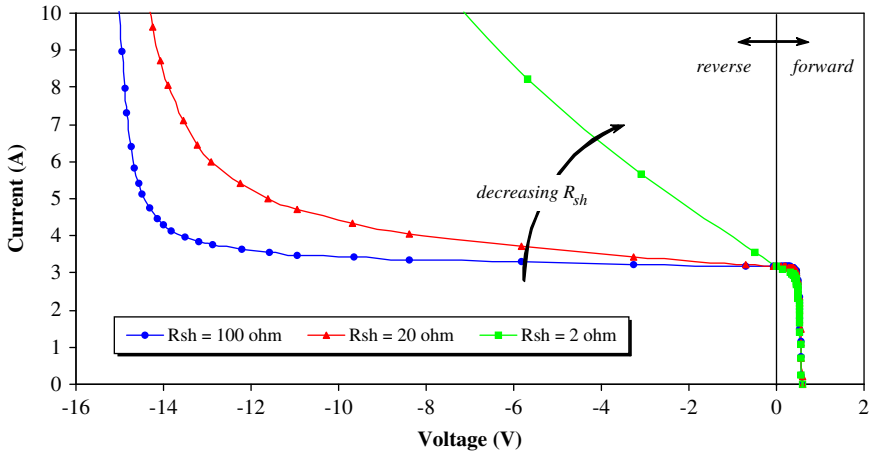

Fig. 1. Illustration of power dissipation due to reduced R_{sh} operating in the reverse mode [8].

Different c-Si cells, which have been observed to have developed a hot-spot have been studied using both EDX and SEM analysis. The hot-spot location has been obtained by an infrared camera.

3. Experimental procedure

c-Si solar cells were subjected to hot-spot checking while in the dark. Seven cells were connected to an external DC source in the reverse mode at 10 V biasing. It should be noted that there was no special selection procedure for the samples in question, due to limited resources. Using IR thermography, areas of high temperatures (hot-spot) were observed. Three cells were observed to have hot-spot areas even though the samples had not been exposed to outdoor operating conditions. The three cells that developed hot-spots were labeled as sample 1, 2 and 3. From each of the three samples, four specimens were prepared for EDX, SEM and Auger electron spectroscopy (AES) analyses. Sample 1 was analyzed after 35 min, sample 2 after 52 min and sample 3 after 43 min. Fig. 3 illustrates how the specimens from each sample were prepared.

Each sample (solar cell) was divided into 3 regions/areas that were classified as hot-spot centre, outside hot-spot and non-hot-spot areas. The same number of specimens was prepared from a sample that did not develop any hot-spot. The sample was prepared for EDX and SEM analysis to observe the possible causes. Specimens used in EDX and SEM analysis were prepared in a manner as follows:

i) Within the hot-spot centre area (~150 °C), 4 specimens were prepared. Specimens were cut starting from the centre of the hot-spot moving away to areas of low temperatures (outside hot-spot areas),
ii) Four specimens (outside hot-spot area) of the same dimensions as the ones inside a hot-spot centre area were prepared.
iii) Specimens were also prepared from one of the cells that did not exhibit hot-spot formation during this test period.

This procedure was followed because as you move away from the hot-spot centre area (characterized by high temperatures), the temperature decreases. From the same areas where the EDX specimens were prepared, four specimens from the hot-spot centre region, four specimens from outside hot-spot region and four specimens from non-hot-spot were prepared for analysis. Two specimens were taken from the control cell for comparison. The procedure followed for AES analysis was to first obtain the Auger spectrum of the sample, then turn ON the ion gun and sputter the surface away, after which another AES spectrum was obtained. Finally the third AES spectrum is obtained after a longer period of sputtering. This procedure was done for all samples used in this study.

4. Results and discussion

4.1. SEM/EDX analysis of a hot-spot region and outside hot-spot

IR images obtained for mc-Si samples exhibited an inhomogeneity of the surface temperatures after 1200 s at reverse bias mode due to localized heating as presented in Fig. 4.

The temperature variation of the cell was monitored. IR images were taken at 300 s intervals. A large part of the cell temperature profile remained constant, exhibiting no signs of overheating. The area circled in Fig. 4(b) and (c) developed localized increase in surface temperature after 1200 s, at which point the maximum temperature profile reached 80 °C. The sample temperature was analyzed again after 3600 s and the observed hot-spot temperature was 150 °C. Fig. 5 illustrates a SEM image of a specimen prepared from a hot-spot centre area of sample 1 when the surface temperature reached 80 °C.

This clearly indicates that focal point heating at the hot-spot site causes irreversible destruction of the solar cell structure. Fig. 6 illustrates the SEM images obtained for sample 2 viewed at 50 μm and the one for the area outside hot-spot. Comparing the area inside the circle of Fig. 6(a) with that outside the circle, it is clear that some damage of the pyramidal structure occurred. This is evidenced by the dark spots indicating a reduced packing density of the surface structure.

It should be noted that all the EDX results presented in this section were taken from the areas of the samples as illustrated in Fig. 3. Fig. 7 shows a typical temperature profile across the cell exhibiting hot-spot formation.

The low-temperature values at the bus bar indicate that the bus bars have relatively higher conductivities, therefore no heat loss is observed.

It is interesting to note that a high temperature area (hot-spot) cannot be precisely identified by merely looking at the sample. However, obtaining a SEM image, surface irregularities on the affected areas are easily identified. Following the procedure used to locate a hot-spot in sample 1, the hot-spot was located in sample 3. Fig. 8 illustrates the SEM image of a hot-spot site located

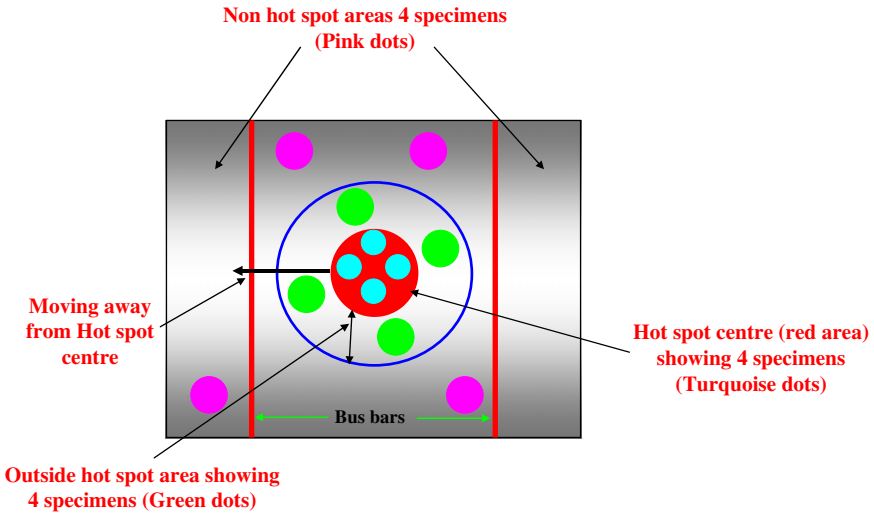

Fig. 3. Illustration of how the specimens were prepared form each sample from different areas.

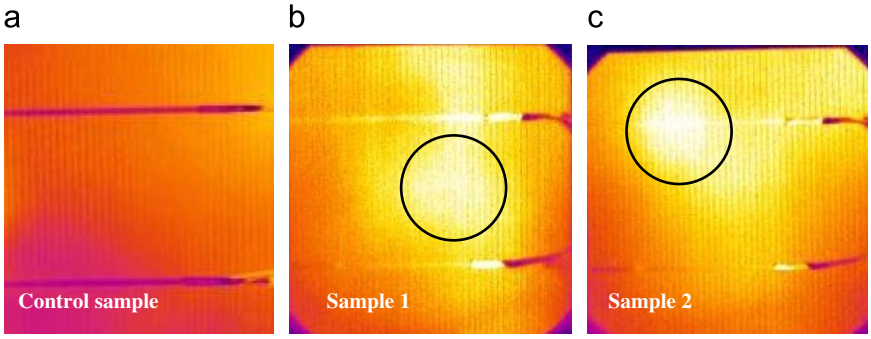

Fig. 4. Hot-spot development in some of the samples used in this experiment (a) no heating, (b) increasing temperature (sample 1), (c) increasing temperature in sample 2. These images were taken from the samples that had been reverse biased for 1200 s.

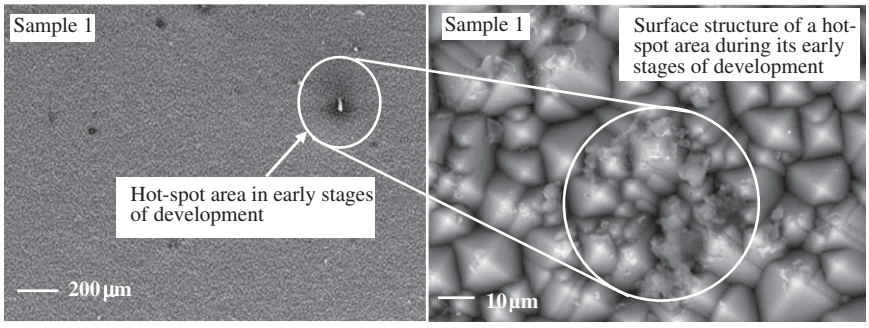

Fig. 5. SEM image of a hot-spot area during its initial stages of development at 200 and 10 µm (sample 1).

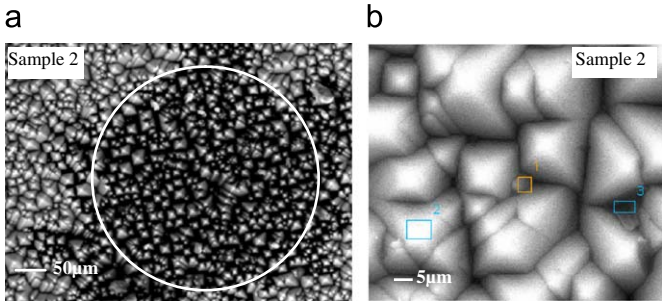

Fig. 6. SEM image of (a) specimen from hot-spot area fully developed at 50 µm for sample 2 at 150 °C and (b) specimen of a non hot-spot area.

in sample 3. This clearly indicates that focal point heating at the hot-spot site causes irreversible destruction of the solar cell structure.

Analyzing closely the temperature profile of sample 3, the heat generated at the hot-spot sight is very high, such that it causes the nearest areas around it including busbar 1 to heat up as well. Moving further away the hot-spot centre, there is a drop in temperature of the cell surface area including busbar 2.

Having identified the samples that developed hot-spots, the specimens of 5 mm × 5 mm from different regions of the sample as illustrated in Fig. 3 were analyzed for the elemental composition using EDX analysis. In brief, EDX is an analytical technique used for identifying the elemental composition or chemical characterization of the specimen or a sample. EDX principle of operation and analysis of the sample is based on an interaction between electromagnetic radiation and the sample, analyzing X-rays emitted by the sample in response of being hit with charged particles. The EDX spectrum displays peaks corresponding to the energy levels (unique to individual atom) for which most X-rays have been received. Fig. 9 shows the EDX profile of the 3 samples prepared from a hot-spot centre area.

Evident from Fig. 9 is the presence of high oxygen content and other metal contaminants for the hot-spot area. Clearly illustrated from sample 2 are the high carbon (C) concentration and a low O complex concentration. The difference in the dominant element at hot-spot sites from different cells fabricated under the same conditions and technique, demonstrates the diversity of the final product that goes into the market. Broadly speaking, all cells encapsulated in a module may have different characteristics and hence have different current producing capabilities. This may result in mismatched conditions, which in turn could result in hot-spot formation. The other well-known element that contributes towards solar cell degradation is iron (Fe) as confirmed by the peak at 4.3 keV in both samples 1 and 3. Notable from Fig. 9 is the change in peak of each element. The change in peak of each element at different accelerating voltages is due to the fact that the electrons that are responsible for the photon emission did not penetrate equally in each sample. The difference in penetration rate of electrons is due to a phase shift as a result of the reaction between transition elements and other elements (in low concentration) that are present in the sample. However, all elements are within their energy range. This clearly shows that areas of high temperature (hot-spot) in mc-Si have high impurities and oxygen complexes.

Moving away from the hot-spot centre area a significant reduction in oxygen, iron and other transition-metals was observed as illustrated in Fig. 10. Fig. 10 illustrates the elementary composition of an area outside hot-spot (cold spot).

Comparing Figs. 9 and 10, it is observed that from regions away from the hot-spot, the impurity concentration starts to decrease

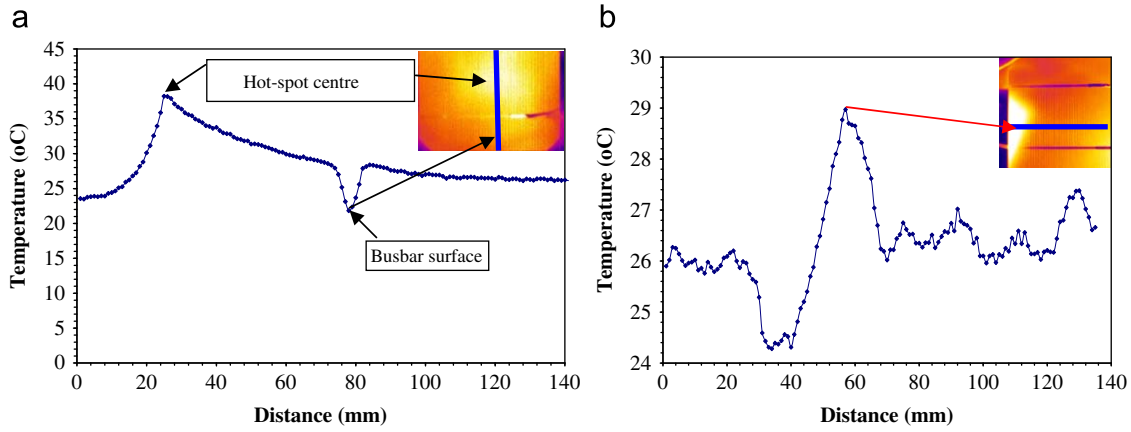

Fig. 7. Temperature profile across cell of the cell Fig. 7 (a) and (b) obtained from IR thermography during the early stages of hot-spot development.

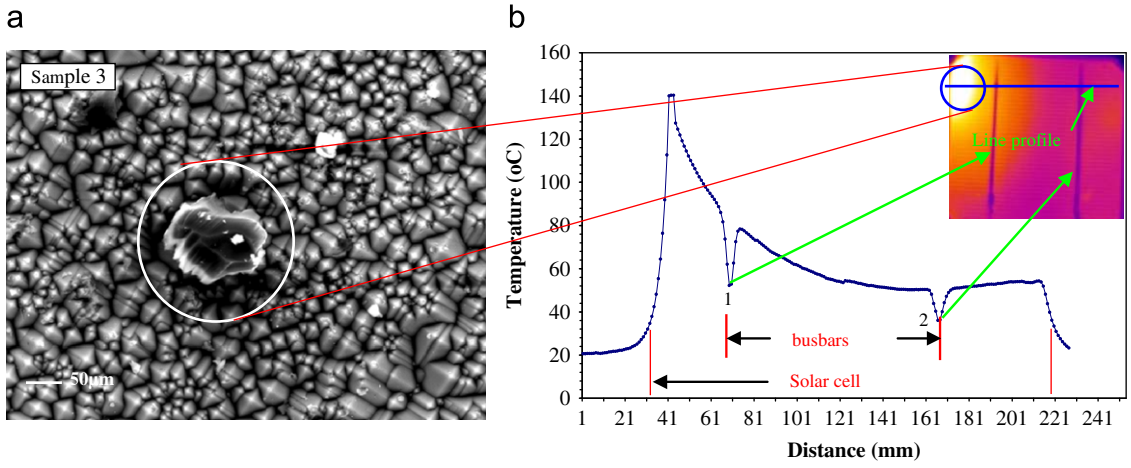

Fig. 8. Effect of focal point heating (hot-spot) leading to total cell destruction, area circled (a) and the corresponding temperature profile (b).

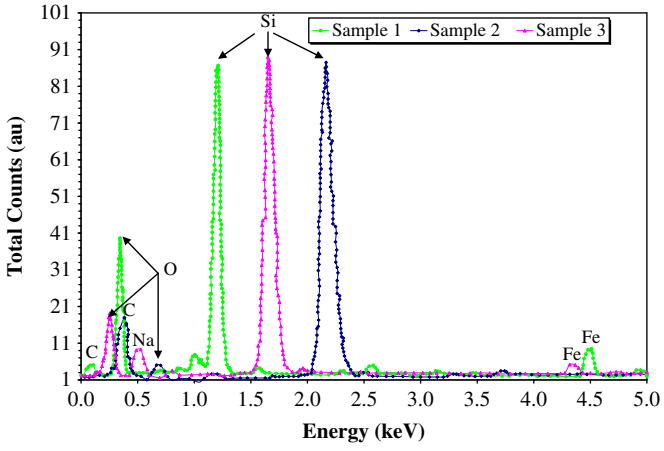

Fig. 9. EDX analysis of hot-spot areas of the 3 samples.

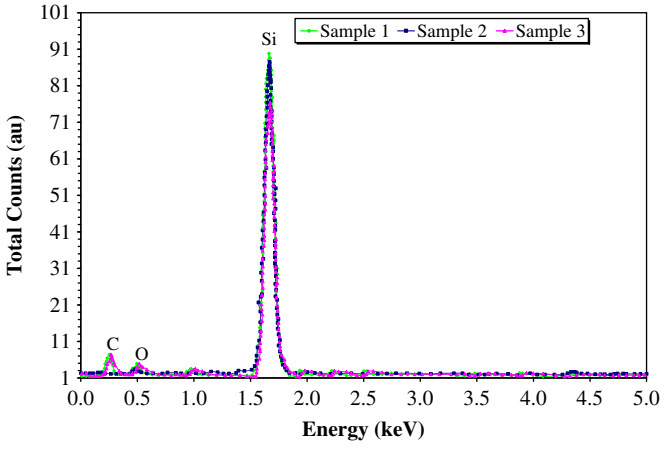

Fig. 10. Elementary composition in areas outside hot-spot region from the 3 samples.

as can be seen by the reduction in oxygen concentration and other transition elements. It is interesting to note that these elements are in different concentrations from one point of the solar cell to the other confirming that the elemental composition of the material is not homogenous. It is noted that oxygen is in relatively low concentrations while iron (Fe) is almost non-existent. Results obtained for all three samples therefore confirm that hot-spot formation is determined by localized elemental composition.

4.2. Auger electron spectroscopy (AES) analysis of a hot-spot region

To further verify the results obtained using EDX for all our samples, a more advanced elemental analysis tool, Auger electron spectroscopy (AES) was used. This was done purely because EDX cannot detect precisely other transition metals present in the samples (e.g., Ti, S and Pt). This is purely because EDX is a surface analytic tool, therefore cannot detect deep level elements as in the

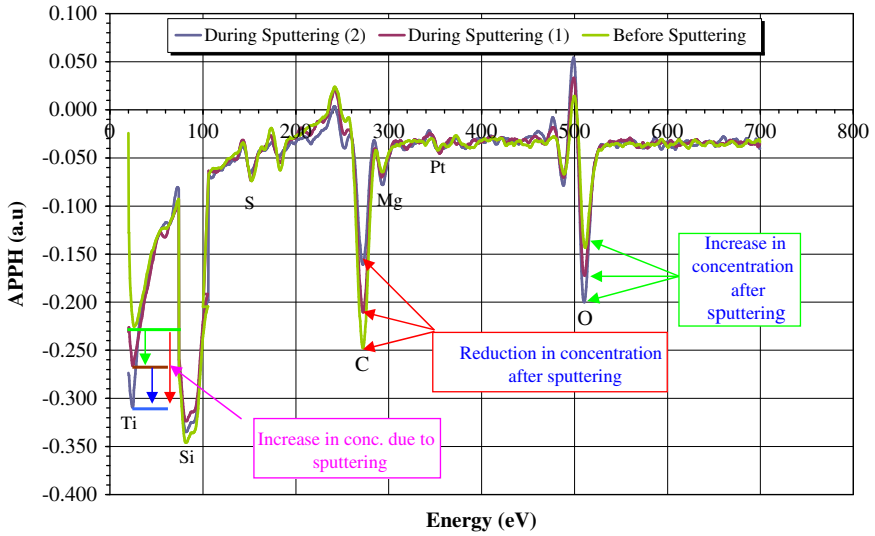

Fig. 11. Auger electron spectrum of the impurity modes at a hot-spot site of a c-Si solar cell.

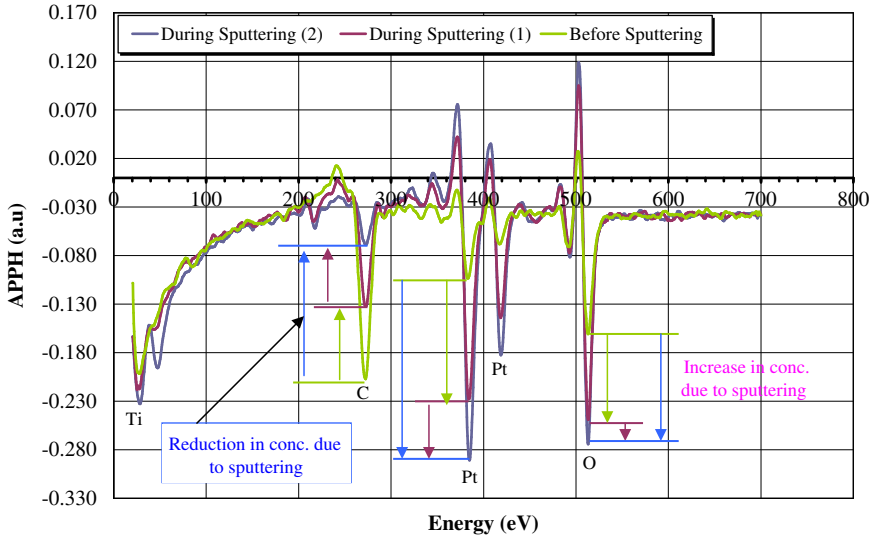

Fig. 12. Auger electron spectrum of sample 2 inside a hot-spot area.

case of AES. The AES unit in the Department of Physics from the University Free State was used.

The procedure for obtaining AES spectrum was to first obtain the AES spectrum of the specimen, sputter the surface away and obtain another spectrum. The 3rd AES spectrum was obtained after a longer period of sputtering. The sputtering rate of 10^{-3} μm/min was used with an interval of 2 min for the first sputtering and 4 min for the second sputtering. This procedure was followed to determine the elemental composition at various depths of the sample. Note that all specimens taken from sample 1 within the hot-spot centre region had the same spectrum, indicating similar elemental composition. This was the case for all sample groups. Therefore only one AES spectrum for each sample will be presented. The Auger peak to peak height (APPH) is an indication of the intensity (absolute value) of the elementary composition. Fig. 11 shows the AES spectrum of an area inside a hot-spot centre area for sample 1.

A high oxygen concentration was detected after the specimen was sputtered twice, which is different from the carbon, whose concentration is higher before sputtering. The increase in Ti and O concentration after sputtering are in high concentration as you move deeper into the sample while C is in low concentration. The increase in concentration as we move deeper into the sample (towards the junction) has an effect on inserting new donor levels in the forbidden band, and results in a free passage for electrons (shunt paths), thereby leading to hot-spot formation. Apart from other elements already detected by EDX analysis, other elements e.g., Pt, S and Ti were detected with high concentration at the hot-spot area from the sample. Figs. 12 and 13 show the elemental composition of sample 2 and sample 3, respectively, using Auger electron spectrum.

From Fig. 12, some elements detected by AES (Ti, Pt and S) could not be detected by EDX profiles. This confirms that indeed these elements are present at the hot-spot area in large concentrations. Also of interest to note is the difference in Pt peaks at different accelerating energy. These shifts of Pt can be explained as follows: Specific incident energy can remove an electron in a particular energy level, resulting in another electron to release energy and occupy this hole. The released energy, which is absorbed by the Auger electron reveals the identity of the atom. Within the same atom, the same process can also occur at another incident energy value where a hole is created in a deeper energy

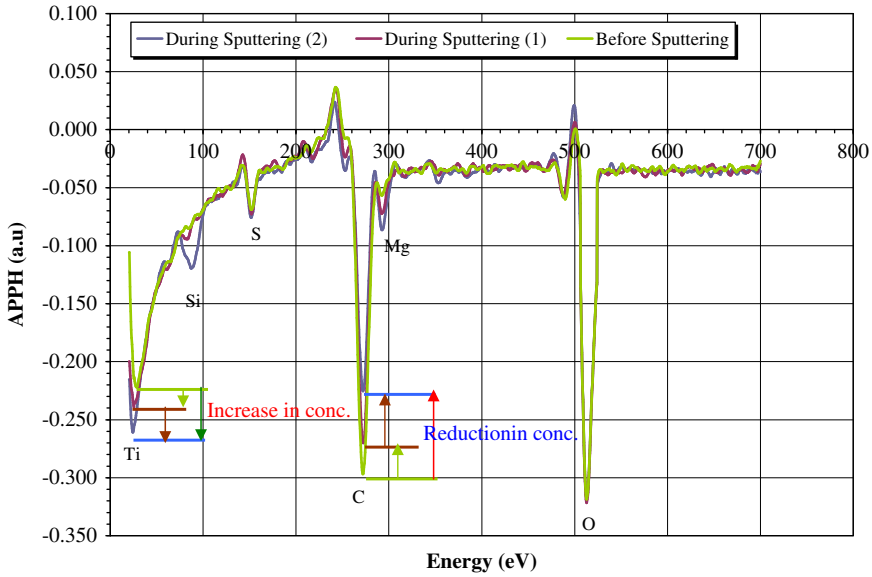

Fig. 13. Auger electron spectrum of sample 3 inside a hot-spot region.

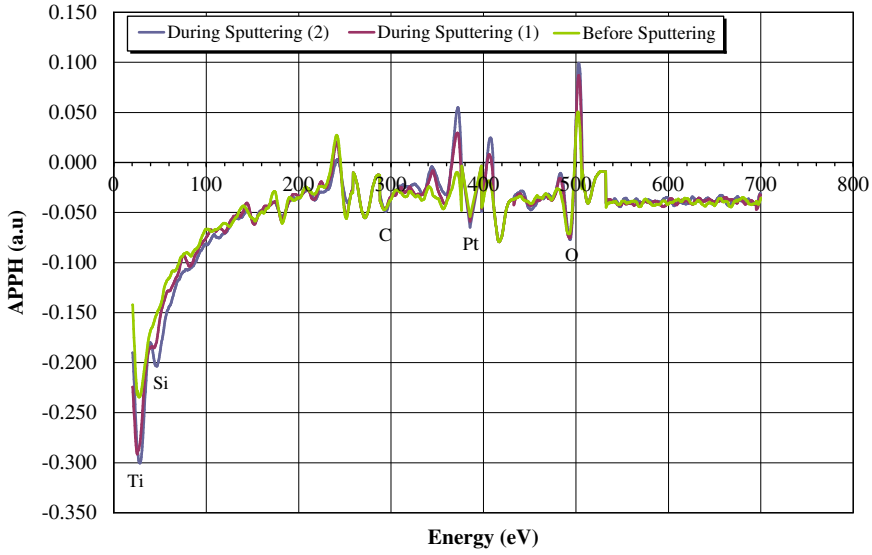

Fig. 14. Auger electron spectrum of the sample out side a hot-spot area spectrum.

level than the previous one. This results in the same element to be identified at different incident energy values. The elemental composition from sample 3 (Fig. 13) reveals the presence of Mg. Oxygen and carbon are found to be in large concentration compared from other samples while very low concentration of Pt was also detected, as opposed to high Pt concentration detected from sample 2. This explains that the extent of the damage to the cell due to the hot-spot that had developed was as a result of the high presence of oxygen and transition elements. Also evident is absence/low concentration of Pt, which was found from other samples. Results from the various areas outside the hot-spot were found to be consistent as indicated in Fig. 14.

Apart from the host element silicon, which is in large concentration, all elements found are in very low concentration. This suggests that the minimum impurity levels due to transition elements in low concentration are not detrimental to the device.

5. Conclusion

Results presented in this work reveal a direct correlation between areas of high impurity contaminants and hot-spot heating in different samples of mc-Si. Elemental concentration in mc-Si solar cells are not homogenously distributed with high concentration of transition metals detected at hot-spot areas. Although several transition elements exist at hot-spot regions, the presence of oxygen, carbon, iron and platinum on these sites, is attributed to the formation of hot-spots in these solar cells. Once again infrared thermography has proved to be the best technique for identifying faults including hot-spot development. Although it might be costly to reduce the concentration of these transitions elements and O complexes by PV manufacturers, it is recommended that transition elements and oxygen must be minimized so as to increase the life expectancy of these devices and overall improve systems reliability.

Acknowledgements

Authors acknowledge the Govan Mbeki Research and Development Centre (GMRC and Eskom Tertiary Education Support Programme (TESP) for their financial support. We also thank The Auger Electron Spectroscopy (AES) unit in the Department of Physics from the University Free State for allowing us to make use of their facility during this study.

References

[1] W. Herrmann, W. Wiesner, W. Waassen, Hot spot investigations on PV modules—new concepts for a test standard and consequences for module design with respect to bypass diodes, in: Proceedings of the 26th IEEE Photovoltaic Specialists Conference, 1997, pp. 1129–1132.
[2] J. Wohlgemuth, W. Herrmann, Reliability testing for PV modules, in: Proceedings of the 29th IEEE Photovoltaic Specialist Conference, 1994, pp. 889–892.
[3] H. Yoshioka, S. Nishikawa, S. Nakajima, M. Asai, S. Takeoka, T. Matsutani, A. Suzuki, Non hot spot PV modules using solar cells with bypass diode function, in: Proceedings of the 25th IEEE Photovoltaic Specialists Conference, 1996, pp. 1271–1274.
[4] D.L. King, J.A. Kratochvil, M.A. Quintana, Application for infrared imaging equipment in photovoltaic cell, modules and systems, in: Proceedings of the 28th IEEE Photovoltaic Specialists Conference, Anchorage, 2000, pp. 1487–1490.
[5] C.C. Gonzalez, R. Liang, R.G. Rosset, Hot spot durability testing of amorphous cells and modules, in: Proceedings of the 18th IEEE Photovoltaic Specialists Conference, 1985, pp. 1041–1046.
[6] L.N. Dumas, A. Shmka, Field failures mechanisms for photovoltaic modules, in: Proceedings of the 15th IEEE Photovoltaic Specialists Conference, 1981, pp. 1091–1098.
[7] J. Wohlgemuth, W. Herrmann, Reliability testing for PV modules, in: Proceedings of the 29th IEEE Photovoltaic Specialist Conference, 1994, pp. 889–892.
[8] E.L. Meyer, On the reliability degradation and failure of photovoltaic modules, University of Port Elizabeth, Ph.D. Thesis, 2002, pp. 74–77, 34–38.
[9] D. Macdonald, A. Cuevas, A. Kinomura, Y. Nakano, Phosphorus gettering in multicrystalline silicon studied by neutron activation analysis, in: Proceedings of the 29th IEEE Photovoltaic Specialists Conference, 2002, pp. 285–288.
[10] D. Macdonald, A. Cuevas, A. Kinomura, Y. Nakano, L.J. Geerligs, Transition-metal profiles in a multicrystalline silicon ingot, Journal of Applied Physics 97 (2005) 033523-1–033523-7.
[11] J. Schmidt, K. Bothe, D. Macdonald, J. Adey, R. Jones, D.W. Palmer, Mechanisms of light-induced degradation in mono- and multicrystalline silicon solar cells, in: Presented at 20th European Photovoltaic Solar Energy Conference, Barcelona, Spain, 2005, pp. 761–764.
[12] O. Breitenstein, J.P. Rakotoniaina, M.H. Rifai, M. Werner, Shunt types in crystalline silicon solar cells, Progress in Photovoltaic: Research and applications 12 (2004) 529–538.
[13] O. Breitenstein, J.P. Rakotoniaina, J. Schmidt, Comparison of shunt imaging by liquid crystal sheets and lock-in thermography, in: Presented at the 12th Workshop on Crystalline Silicon Solar cells Material and Processing, Colorado, 2002.
[14] T. Buonassisi, O.F. Vyvenko, A.A. Istratov, E.R. Weber, Observation of transition metals at shunt locations in multicrystalline silicon solar cells, Journal of Physics 95 (2004) 1556–1561.